

1 Helm Glacier projected to vanish within a decade

2 Jeffrey W. CROMPTON¹, Brian MENOUNOS^{1,3,4}, Mark EDNIE²

3 ¹*Geological Survey of Canada, Natural Resources Canada, Vancouver, British Columbia, Canada*

4 ²*Geological Survey of Canada, Natural Resources Canada, Ottawa, ON, Canada,*

5 ³*Department of Geography, Earth, and Environmental Science, University of Northern British Columbia,*
6 *Prince George, British Columbia, Canada*

7 ⁴*Hakai Institute, Campbell River, British Columbia, Canada*

8 **ABSTRACT.** Goodbye Helm, thanks for all the ice

9 INTRODUCTION

10 Over the last four years, glaciers in Western Canada and the conterminous US lost twice as much mass
11 as during the period 2010-2019 (Menounos and others, 2025). This mass loss occurred primarily through
12 widespread surface thinning driven by warm, dry conditions and general darkening of glacier surfaces. In
13 terms of surface area, Canada contains about 185,000 km² of glacierized terrain, about one quarter of the
14 global total (Consortium, 2023). Given the importance of glacier runoff to Canada's economy, the federal
15 government established a network of glacier monitoring sites during the International Hydrological Decade
16 (IHD) (Ommeney, 1986). These sites became operational in 1965 and, ten years later, the Government
17 of Canada added Helm Glacier to its list of monitoring sites given its maritime environment (Ommeney
18 and others (2002)). Helm Glacier is a World Glacier Monitoring Service (WGMS) reference glacier and
19 only one of four alpine glaciers in Canada to have monitoring record which exceeds 40 years. In addition to
20 their importance of recording seasonal-to-annual response of glaciers to climate change, in situ glacier
21 monitoring records provides seasonal-to-annual observations required for regional upscaling of glacier mass
22 change (Zemp and others, 2019). The objectives of this short note is to describe recent changes of Helm
23 Glacier and estimate when Helm Glacier is projected to disappear.

24 STUDY AREA AND METHODS

25 Helm Glacier ($49^{\circ}57'29''$ N, $122^{\circ}59'13''$ W) lies on the western edge of Garibaldi Provincial Park in the
26 Pacific Ranges of the southern Coast Mountains in the traditional territory of the Squamish Nation (Figure
27 1). The small (0.4 km^2) glacier's currently ranges in elevation from 1780 m a.s.l. to 2150 m a.s.l.

28 Glacier mapping mass balance surveys

29 We digitized the extent of Helm Glacier from spaceborne (Landsat 5,7,8,9) and airborne ortho-imagery,
30 the latter acquired by the Hakai-UNBC Airborne Coastal Observatory (Donahue and others, 2023). We
31 take the product of the ground sampling distance of the imagery and the glacier's perimeter to reflect
32 the uncertainty in our mapping. As described above, Helm Glacier represents a WGMS reference glacier
33 where mass balance measurements follow the stratigraphic method (Kaser and others, 2003). The glacier's
34 seasonal balances are derived from 6-8 ablation stakes positioned along the centreline of the glacier, snow
35 depth probing and end-of-winter snow pits where snow density and stratigraphic observations are made.
36 Those data are used to generate seasonal and annual mass balance for the glacier and by updating the
37 glacier area every few years.

38 Ice-penetrating radar

39 We completed an ice-penetrating radar survey of Helm Glacier on 21 May, 2025. The Blue Systems
40 Integration Ltd. radar system uses resistively-loaded dipole antennas with a centre frequency of 10 MHz,
41 has 12-bit resolution and yields a sampling rate of up to 250 Megasamples per second. The radar system
42 contains a single frequency GNSS system with an accuracy of $\pm 5 \text{ m}$. To increase the vertical accuracy
43 for the glacier surface ($\pm 0.5 \text{ m}$), we acquired airborne Lidar for the surface elevation of the glacier on
44 24 April, 2025. Details about methods used for Lidar acquisition can be found elsewhere (Menounos and
45 others, 2025). Observations of surface elevation change from a sonic depth ranger equipped with satellite
46 telemetry Bevington and others (2025), reveals about 1 m of thinning between our Lidar and radar surveys.
47 We processed the radar data with IceRadarAnalyzer 6.3.1, with an antenna spacing of 15 m and assuming
48 a velocity through ice at $1.68 \times 10^8 \text{ m s}^{-1}$ (Reynolds, 2011). To increase the signal-to-noise ratio of the data,
49 we averaged 128 stacks for each trace in the radargram and then applied gain and filtering for identification
50 of bed reflectors. We completed crossover analysis (i.e. where two radar transects overlap) and propagated
51 in quadrature the uncertainty using one-quarter of the radar wavelength Reynolds (2011) and uncertainty

52 that arises from surface slope to yield an error of ice thickness of ± 4.5 m. 2D linear interpolation of the
 53 ice thickness data yielded a map of ice thickness (10 m ground sampling distance - gsd).

54 Projection of glacier disappearance

55 To estimate when Helm Glacier is expected to vanish, we forward model the yearly surface elevation change
 56 of Helm Glacier using two approaches described below. Both of these approaches use surface elevation data
 57 obtained from repeat Lidar surveys of Helm Glacier completed at the end of ablation season in 2020–2024.
 58 These five autumn surveys provide elevation change maps for 2021, 2022, 2023 and 2024. Those airborne
 59 surveys followed the same methods as those used for the 24 April, 2025 survey. As described below, elevation
 60 change at a given point can be equated to annual surface mass balance given the thinness of the glacier (i.e.
 61 negligible dynamics) and minimal extent of retained snow on the glacier (i.e. density-to-mass conversion
 62 is simplified). The elevation change maps are downsampled to 10 m gsd to match the ice thickness grid.
 63 Co-registration of elevation change maps used methods described in Nuth and Kääb (2011) and Hugonet
 64 and others (2022) available in the XDEM package (<https://pypi.org/project/xdem/>).

65 Our first approach averages the surface elevation change at each grid cell over the four year period,
 66 then simply differences this average elevation change from the ice thickness grid each year (method 1). Ice
 67 vanishes at a given grid cell when the total melt exceeds the ice thickness of the column. The error in area
 68 is simply taken recomputing the elevation change within the ice thickness error bounds of 4.5 m.

69 For the second approach, we use a regression model to predict elevation change \mathbf{dh}^y based on the design
 70 matrix of observations \mathbf{X}^y for each of the years $j = \{2021, 2022, 2023, 2024\}$ for each of the n grid cells
 71 (method 2). Linear regression can be used to model mass change at the regional (Lliboutry, 1974; Anilkumar
 72 and others, 2023; Reynaud and others, 1986) to individual ablation stake scale (Zekollari and Huybrechts,
 73 2018). The matrix \mathbf{X}^y is composed of slope ($\boldsymbol{\theta}^y$), orientation ($\boldsymbol{\alpha}^y$), positive-degree days (\mathbf{PDD}^y), shortwave
 74 radiation at the surface ($\mathbf{SW}_{\downarrow}^y$) and snow depth (\mathbf{h}^y). The regression $\mathbf{dh} = \mathbf{X}\boldsymbol{\beta} + \boldsymbol{\epsilon}$ is computed on the
 75 matrix \mathbf{X} and observations \mathbf{dh} that are concatenated across the four-year record. The optimal coefficients
 76 are estimated through least-squares regression as, $\hat{\boldsymbol{\beta}} = (\mathbf{X}^\top \mathbf{X})^{-1} \mathbf{X}^\top \mathbf{M}$. The model is validated by modelling
 77 the surface change for each year individually as $\hat{\mathbf{M}}^j = \mathbf{X}^j \hat{\boldsymbol{\beta}}$, with the R^2 computed between the yearly
 78 difference in observed and modelled elevation change at each grid cell.

79 PDDs are computed are summed in the time intervals given by the LiDAR acquisition dates as
 80 $\mathbf{PDD}^y = \frac{1}{24} \sum T(z)$ for $T > 0^\circ\text{C}$. The temperature (T) is taken from dynamically downscaled hourly
 81 ERA-5 land temperatures (Hersbach and others, 2020) given at the nearest grid point and lapsed up from

82 1550 m to the elevation of each grid cell. Similar to the melt-season lapse rate computed by Shea and
83 others (2009) of $-6.0^{\circ}\text{C km}^{-1}$, we calculate April to October lapse rates from a series of nearby weather
84 stations as $-5.8^{\circ}\text{C km}^{-1}$. Snow depth is estimated from yearly snow depth observations collected every April
85 at six glacier centreline stake locations. A yearly snow depth field is computed as a function of elevation
86 by linearly interpolating observations to grid cell elevations. The summer incoming shortwave radiation
87 is computed by multiplying a shading factor matrix computed in the HORAYZON v1.2 model (Steger
88 and others, 2022) with the mean of the daily averaged downwelling shortwave radiation obtained from the
89 nearest gridpoint of ERA5-Land reanalysis. Although the shading model and surface normal shortwave
90 radiation both depend on surface slope and aspect, we include slope and aspect as individual columns in
91 the design matrix to capture other mass balance processes like snow redistribution.

92 To forward model the ice loss, we start with the 2024 DEM and force the model with the average of the
93 PDD fields from 2014 to 2024, all computed at the 2024 grid cell elevations from April 01 to October 31.
94 The forcing for \mathbf{SW}_{\downarrow} and the snow depth field \mathbf{h} field are generated from averaging the 2020–2024 fields
95 used in the regression model. At each step forward in time, we recompute the surface elevation, slope,
96 aspect, **PDD** field and snow-depth field, but keep \mathbf{SW}_{\downarrow} fixed in time. We estimate uncertainty in elevation
97 change by initializing the ice thickness at the ± 4.5 m error bounds and by varying the lapse rate by $\pm 5\%$.

98 Mass balance sensitivity

99 We test the net mass balance (b_n) sensitivity of our model to changes in temperature as $C_T = \partial b_n / \partial T$ and
100 precipitation as $C_P = \partial b_n / \partial P$. Sensitivities are computed by varying the mean summer temperature and
101 the mean winter accumulation of the model (e.g. Cuffey and Paterson, 2010). Numerical derivatives for C_T
102 and C_P are computed for the current temperature and accumulation conditions. We test the sensitivity
103 of i) yearly specific mass balance using the 2024 reference surface (e.g. Elsberg and others, 2001) and ii)
104 integrated mass balance by allowing the accumulation area to grow from the 2024 reference surface. In
105 the forward model for sensitivity, PDDs are calculated at each grid cell for each incremental temperature
106 change, whereas changes in winter accumulation are input directly into the regression equation. To convert
107 elevation change to mass loss in m w.e., cells with negative elevation change are multiplied by an ice density
108 factor of 0.917. Positive elevation changes indicative of snow accumulation are multiplied by a density factor
109 of 0.41, which is the integrated snow pit density averaged from up to two pit locations per year from 14
110 years of spring surveys dating back to 1997. We compute the percent change in temperature by normalizing
111 by the mean ERA5-Land summer temperature at the mean elevation of the glacier from 2014–2024. The

percent change in accumulation is computed by normalizing the offset in accumulation by the glacier-wide average snow depth field used in the forward model. We compare our modelled temperature sensitivities to observed sensitivities at Helm glacier, computed as the slope of the regression between ERA5-Land mean summer temperature and net specific mass balance from 1975 to 2024 from glaciological mass balance data (WGMS, 2024).

RESULTS

Helm Glacier reached a maximum Holocene areal extent (4.5 km^2) during the Little Ice Age at about 1690–1710 CE (Koch and others, 2009). Except for period of slowed recession with a minor advance between the late 1960's and 1970's, Helm Glacier experienced widespread thinning and attendant shrinkage throughout the Twentieth Century (Koch and others, 2009). Between 1928 and 2024, Helm Glacier lost about 90 % of its surface area with much of this loss appearing after 2010 (Figure 2). Pronounced retreat and thinning over the eight years led to fragmentation of the glacier in its uppermost elevations. Marginal retreat along the glacier's mid section will split the lower and upper portions of the glacier within a year or two (Figure 1).

Since 1975, Helm Glacier experienced only five years of positive mass balance (WGMS, 2024). Recent imagery of the glacier reveals widespread loss of firn with negligible accumulation area especially over the last four years. Glaciological mass balance data averaged over the past seven years show an annual balance at the terminus of -3.6 m w.e. and -1.6 m w.e. at the summit. During that time period, the yearly accumulation averaged over the entire glacier was 1.85 m w.e. From 1984 to present, Helm Glacier experiences the most negative mass balance of all 16 WGMS monitored glaciers in North America (WGMS, 2024). The 2023 melt year was a record breaking loss for Helm Glacier, with a glacier wide annual mass balance of -4.34 m w.e., roughly 2.5 times higher than the average of the previous six years (Menounos and others, 2025).

The change in glacier area through time is largely controlled by the basin geometry, as exemplified by the rapid drop in area in the late 1980s as thin ice in the upper basin vanishes (Fig. 2). Regional trends in accelerated area and mass loss around 2010 (Bevington and Menounos, 2022; Menounos and others, 2019) and again in 2020 (Menounos and others, 2025) cannot be easily distinguished at Helm, though Helm glacier undergoes accelerating area loss that continues from 2014 to present, which does not appear to be controlled by the basin geometry.

Our projections of surface elevation change indicate that Helm glacier will vanish before 2040 (Figs. 2 and 3). Helm glacier is forecast to decrease into fragmented patches of less than 0.1 km^2 by 2028 ± 0.5 (method 1)

142 or by 2029 ± 0.5 (method 2). Projected area loss patterns are controlled predominately by the remaining ice
143 thickness rather than elevation, orientation and slope. A simple extrapolation of the net elevation change
144 field (method 1) yields a more conservative estimate than the linear regression (method 2). For the linear
145 regression, the R^2 is 0.83 and $\hat{\beta}$ values are all statistically significant with $p < 0.001$, with the exception of
146 $\hat{\beta}$ for \mathbf{SW}_\downarrow at $p = 0.065$. Given that slope and aspect account for the greatest spatial variation in incoming
147 shortwave radiation, omitting the \mathbf{SW}_\downarrow and snow accumulation fields from the design matrix can lead to
148 model fits for the 2020–2021 and 2023–2024 melt years with $R^2 \sim 0.7$. However, the reanalysis masked
149 shortwave data are needed to adequately model the high melt season of 2022–2023. Similarly, the design
150 matrix needs to include snow accumulation data to adequately fit the high snow accumulation season
151 of 2021–2022. Relative to the uncertainty in ice depth, the regression model shows little sensitivity to a
152 variation in lapse rate of $\pm 5\%$.

153 Calculating the specific balance from the 2024 reference surface shows that a net-zero balance can be
154 achieved with an increase in precipitation of 1.5 m w.e. (36% mean winter snow accumulation) at the current
155 temperature, or a change in temperature of -6.8°C (95% mean winter snow accumulation) at the current
156 accumulation (Fig. 4 a). By allowing the accumulation area to grow we compute a volumetric balance
157 sensitivity that is slightly more optimistic (Fig. 4 b), requiring an increase in precipitation of 1.1 m w.e.
158 (28%) at the current temperature, or a change in temperature of -5.1°C (71%).

159 For current conditions at Helm glacier, we compute a sensitivity to temperature as
160 $C_T = -0.65 \text{ m w.e. yr}^{-1} \text{ }^\circ\text{C}^{-1}$ while the sensitivity to accumulation is $C_P = 0.97 \text{ m w.e. yr}^{-1} \text{ m w.e.}^{-1}$.
161 On a unit-by-unit basis, the glacier is therefore 1.5 times more sensitive to changes in winter accumulation
162 relative to changes in mean summer temperature. However, comparing the sensitivities by percentage
163 change yield $C_P/C_T = 0.84$. The mass balance sensitivities for both the volumetric and specific mass
164 balance methods yield very similar results. Our modelled value of $C_T = -0.65 \text{ m w.e. yr}^{-1} \text{ }^\circ\text{C}^{-1}$ is in
165 agreement to the observed mass balance temperature sensitivity of $C_T = -0.64 \text{ m w.e. yr}^{-1} \text{ }^\circ\text{C}^{-1}$.

166 DISCUSSION

167 Both methods for projecting surface elevation change lead to a demise of Helm Glacier within the next
168 decade. Applying the average elevation change forward in time (method 1) is slightly more conservative
169 than the regression model (method 2) because surface parameters like slope, orientation and elevation
170 that are updated at each yearly time step in the regression model create a positive feedback in melt rate,
171 which is not captured with the simple extrapolation. Like most glaciers, Helm glacier exhibits several

intricacies that complicate a simple mass balance model or regression approach. For each melt season, modelled surface elevation change is generally underestimated along patches of the eastern margin where avalanche accumulation is exacerbated by valley wall shading. Elevation change is often overestimated at the eastern head of the glacier where snow redistribution by wind causes a reversal of the accumulation gradient. Linearly interpolating and extrapolating snow depth measurements to the snow depth field yields the best R^2 averaged across all observation periods, but in cases of extreme years for snow redistribution, a second or third-order polynomial fit can significantly increase the fit at high and low elevations for that year. Despite the uncertainties in ice thickness and nuances in melt, the glacier is thinning so rapidly that capturing subtleties in mass balance becomes increasingly irrelevant when trying to model the timing of extinction.

The linear regression model is driven by average temperatures over the past decade and an average snow accumulation field. As such, the forward model does not capture extreme melt events observed regionally and at Helm glacier. Examples of events and processes that likely make our projections conservative include the intense melt year of 2023 (Menounos and others, 2025), an equilibrium-line elevation that is starting to rise above the head of the glacier (Bevington and Menounos, 2025), surface darkening from wildfire ash deposition that decreases ice albedo (Menounos and others, 2025; Aubry-Wake and others, 2022) and proglacial lake development leading to basal melt and calving (Carrivick and Tweed, 2013; Shugar and others, 2020). These processes that we do not account for should lead to an overestimate of the temperature shift required to reach equilibrium mass balance (see Fig. 4). However, the temperature shifts that we derive in the sensitivity analyses are consistent with the observed increase in mean summer temperature of 4.6°C from 1950 to present at the nearest ERA5-Land grid point. ERA5-Land reanalysis data does not show a statistically significant increase in precipitation that would otherwise contribute to the magnitude of disequilibrium for Helm glacier.

CONCLUSION

REFERENCES

- Anilkumar R, Bharti R, Chutia D and Aggarwal SP (2023) Modelling point mass balance for the glaciers of the Central European Alps using machine learning techniques. *The Cryosphere*, **17**(7), 2811–2828
- Aubry-Wake C, Bertoncini A and Pomeroy JW (2022) Fire and ice: The impact of wildfire-affected albedo and irradiance on glacier melt. *Earth's Future*, **10**(4), e2022EF002685

- 201 Bevington AR and Menounos B (2022) Accelerated change in the glaciated environments of western Canada revealed
202 through trend analysis of optical satellite imagery. *Remote Sensing of Environment*, **270**, 112862
- 203 Bevington AR and Menounos B (2025) Glaciers in western North America experience exceptional transient snowline
204 rise over satellite era. *Environmental Research Letters*, **20**(5), 054044
- 205 Bevington AR, Menounos B and Ednie M (2025) Satellite telemetry of surface ablation observations to inform spatial
206 melt modelling, Place Glacier, British Columbia, Canada. *EGUphere*, **2025**, 1–30
- 207 Carrivick JL and Tweed FS (2013) Proglacial lakes: character, behaviour and geological importance. *Quaternary
208 Science Reviews*, **78**, 34–52
- 209 Consortium R (2023) Randolph glacier inventory-a dataset of global glacier outlines, version 7. *NASA National Snow
210 and Ice Data Center Distributed Active Archive Center (DAAC) data set*, F6JMOVY5NAVZ
- 211 Cuffey KM and Paterson WSB (2010) *The physics of glaciers*. Academic Press
- 212 Donahue CP, Menounos B, Viner N, Skiles SM, Beffort S, Denoudin T, Arriola SG, White R and
213 Heathfield D (2023) Bridging the gap between airborne and spaceborne imaging spectroscopy for mountain
214 glacier surface property retrievals. *Remote Sensing of Environment*, **299**, 113849, ISSN 0034-4257 (doi:
215 <https://doi.org/10.1016/j.rse.2023.113849>)
- 216 Elsberg D, Harrison W, Echelmeyer K and Krimmel R (2001) Quantifying the effects of climate and surface change
217 on glacier mass balance. *Journal of Glaciology*, **47**(159), 649–658
- 218 Hersbach H, Bell B, Berrisford P, Hirahara S, Horányi A, Muñoz-Sabater J, Nicolas J, Peubey C, Radu R, Schepers
219 D and others (2020) The ERA5 global reanalysis. *Quarterly journal of the royal meteorological society*, **146**(730),
220 1999–2049
- 221 Hugonnet R, Brun F, Berthier E, Dehecq A, Mannerfelt ES, Eckert N and Farinotti D (2022) Uncertainty analysis
222 of digital elevation models by spatial inference from stable terrain. *IEEE Journal of Selected Topics in Applied
223 Earth Observations and Remote Sensing*, **15**, 6456–6472
- 224 Kaser G, Fountain A and Jansson P (2003) *A Manual for Monitoring the Mass Balance of Mountain Glaciers*.
225 UNESCO, Paris
- 226 Koch J, Menounos B and Clague JJ (2009) Glacier change in Garibaldi Provincial Park, southern Coast Mountains,
227 British Columbia, since the Little Ice Age. *Global and Planetary Change*, **66**(3-4), 161–178
- 228 Lliboutry L (1974) Multivariate statistical analysis of glacier annual balances. *Journal of Glaciology*, **13**(69), 371–392
- 229 Menounos B, Hugonnet R, Shean D, Gardner A, Howat I, Berthier E, Pelto B, Tennant C, Shea J, Noh MJ and
230 others (2019) Heterogeneous changes in western North American glaciers linked to decadal variability in zonal
231 wind strength. *Geophysical Research Letters*, **46**(1), 200–209

- 232 Menounos B, Huss M, Marshall S, Ednie M, Florentine C and Hartl L (2025) Glaciers in Western Canada-
233 conterminous US and Switzerland experience unprecedented mass loss over the last four years (2021–2024).
234 *Geophysical Research Letters*, **52**(12), e2025GL115235
- 235 Nuth C and Kääb A (2011) Co-registration and bias corrections of satellite elevation data sets for quantifying glacier
236 thickness change. *The Cryosphere*, **5**(1), 271–290
- 237 Ommannay C (1986) Mapping Canada's glaciers since 1965. *Annals of glaciology*, **8**, 132–134
- 238 Ommannay C, Demuth M and Meier M (2002) Glaciers of North America. *US Geological Survey Professional Paper*,
239 **1386**, 23
- 240 Reynaud L, Vallon M and Letreguilly A (1986) Mass-balance measurements: problems and two new methods of
241 determining variations. *Journal of Glaciology*, **32**(112), 446–454
- 242 Reynolds JM (2011) *An introduction to applied and environmental geophysics*. John Wiley & Sons
- 243 Shea JM, Moore RD and Stahl K (2009) Derivation of melt factors from glacier mass-balance records in western
244 Canada. *Journal of Glaciology*, **55**(189), 123–130
- 245 Shugar DH, Burr A, Haritashya UK, Kargel JS, Watson CS, Kennedy MC, Bevington AR, Betts RA, Harrison S and
246 Strattman K (2020) Rapid worldwide growth of glacial lakes since 1990. *Nature climate change*, **10**(10), 939–945
- 247 Steger CR, Steger B and Schär C (2022) HORAYZON v1. 2: an efficient and flexible ray-tracing algorithm to compute
248 horizon and sky view factor. *Geoscientific Model Development*, **15**(17), 6817–6840
- 249 WGMS (2024) Fluctuations of glaciers database. World Glacier Monitoring Service, Zurich, Switzerland. (doi:
250 10.5904/wgms-fog-2024-07)
- 251 Zekollari H and Huybrechts P (2018) Statistical modelling of the surface mass-balance variability of the Morteratsch
252 glacier, Switzerland: strong control of early melting season meteorological conditions. *Journal of Glaciology*,
253 **64**(244), 275–288
- 254 Zemp M, Huss M, Thibert E, Eckert N, McNabb R, Huber J, Barandun M, Machguth H, Nussbaumer SU, Gärtner-
255 Roer I, Thomson L, Paul F, Maussion F, Kutuzov S and Cogley JG (2019) Global glacier mass changes and their
256 contributions to sea-level rise from 1961 to 2016. *Nature*, **568**(7752), 382–386

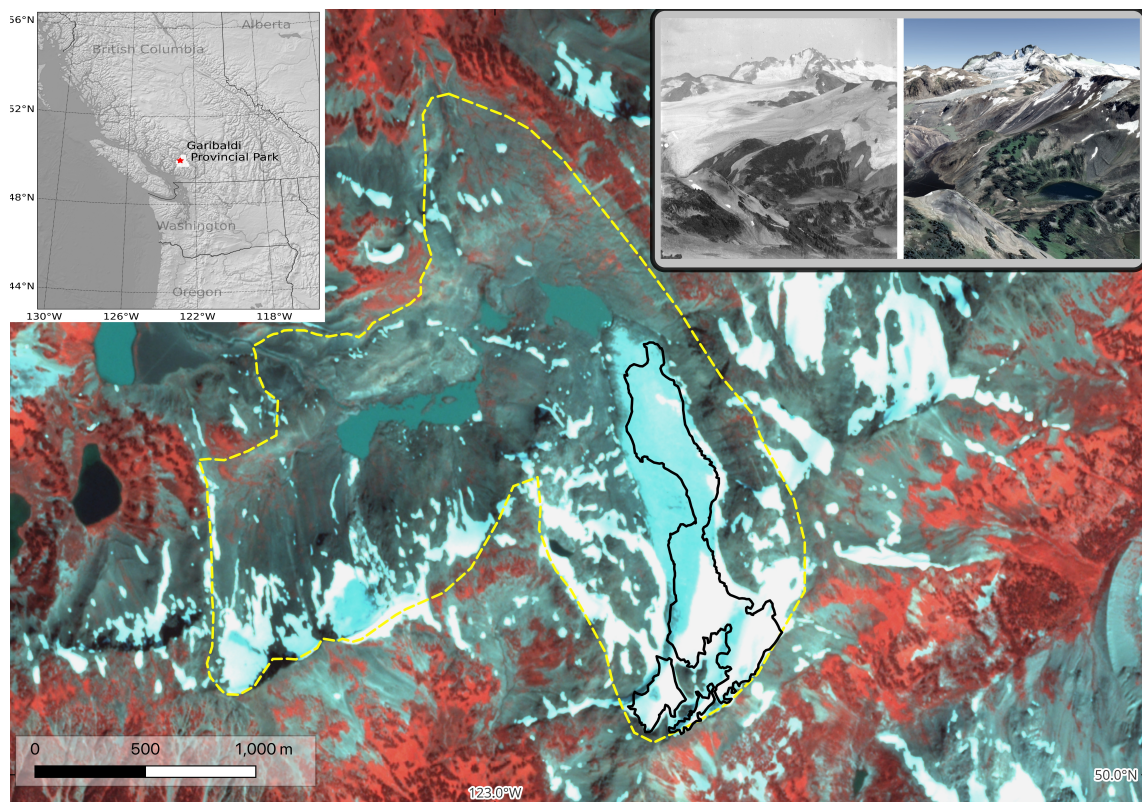


Fig. 1. **Inset map:** Helm Glacier (red star) within Garibaldi Provincial Park. **Background image:** PlaceScope color composite (NIR-R-G) of Helm Glacier [28 August, 2017] and surrounding terrain. Black solid and yellow dashed lines respectively denote glacier extent in 2024 and 1928 survey photo-topographic survey of the glacier (Koch and others, 2009). **Upper right images:** Oblique image (left) of Helm Glacier in 1910s (unknown photographer) and glacier extent from Google Earth Engine (6 Aug, 2019 imagery). 1910s image courtesy of City of Vancouver Archives

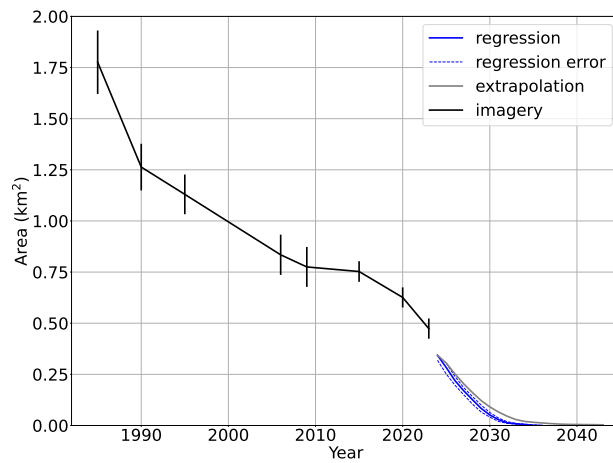


Fig. 2. Modelled and observed glacier area change through time. Vertical bars are uncertainty in area as the product of the image resolution and glacier area. Results for the regression analysis (blue line) are bracketed by initializing the model with the error bounds on ice thickness. Error bounds for the elevation change extrapolation (gray line) are not shown, but are similar in spread to the regression uncertainty.

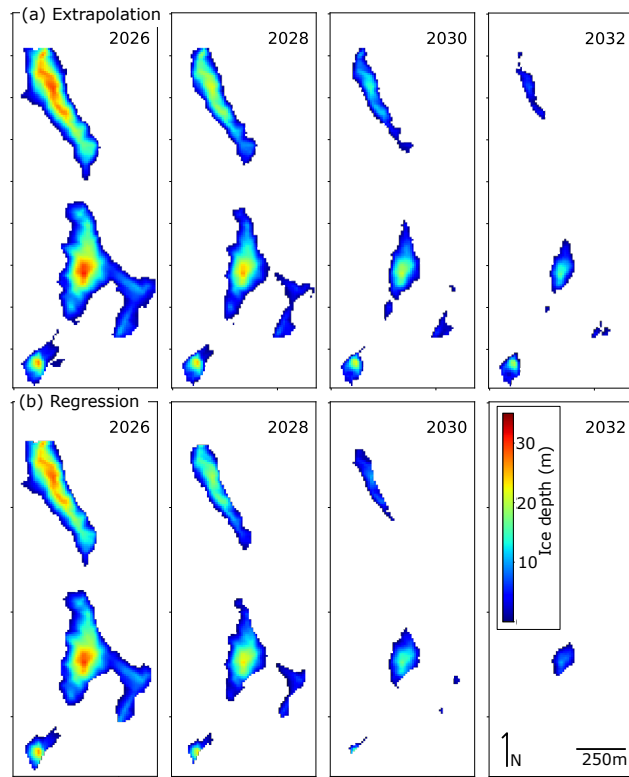


Fig. 3. Forward model of glacier area and thickness by (a - top panels) extrapolation of mean elevation change field between 2020 and 2024 and (b - bottom panels) multivariate regression.

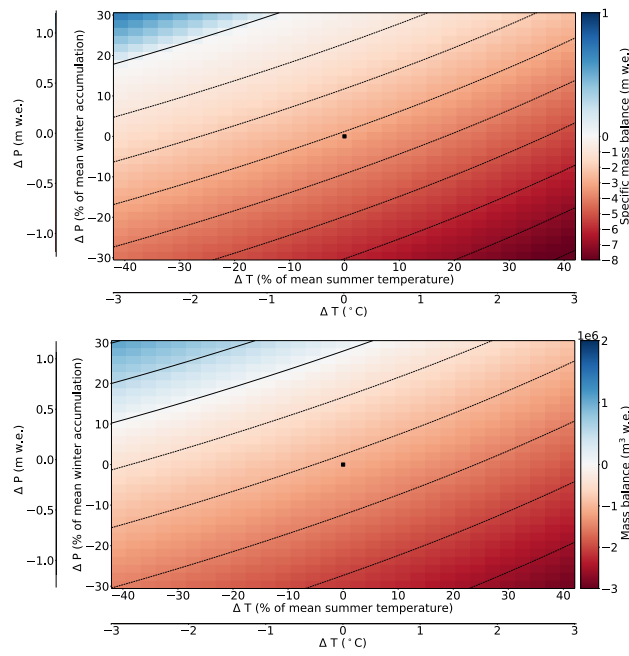


Fig. 4.